Chapter 10
Strong Focusing Synchrotron

Abstract This Chapter introduces the strong focusing synchrotron, alternating gradient (AG) and separated focusing, and the theoretical material needed for the simulation exercises. It begins with a brief reminder of the historical context, and continues with beam optics, chromaticity, and acceleration. It relies on basic charged particle optics and acceleration concepts introduced in the previous Chapters, and further addresses the following aspects:
- resonances and resonant extraction,
- stochastic energy loss by synchrotron radiation.

The simulation of a strong focusing synchrotron requires just two, possibly three, optical elements from `zgoubi` library: DIPOLE, BEND, or MULTIPOL to simulate (possibly combined function) dipoles, DRIFT to simulate straight sections, and MULTIPOL to simulate lenses (which can be otherwise simulated using QUADRUPO, SEXTUPOL, OCTUPOLE, etc.). A fourth element, CAVITE, is required for acceleration. Particle monitoring requires keywords introduced in the previous Chapters, including FAISCEAU, FAISTORE, possibly PICKUPS, and some others. Spin motion computation and monitoring resort to SPNTRK, SPNPRT, FAISTORE. Optics matching and optimization use FIT[2]. INCLUDE is used, mostly here in order to shorten the input data files. SYSTEM is used to, mostly, resort to gnuplot so as to end simulations with some specific graphs obtained by reading data from output files such as zgoubi.fai (resulting from the use of FAISTORE), zgoubi.plt (resulting from IL=2), or other zgoubi.*.out files resulting from a PRINT command.

Notations used in the Text

B; $\mathbf{B}$, $B_{\mathrm{x,y,s}}$	field value; field vector, its components in the moving frame
$B\rho = p/q$; $B\rho_0$	particle rigidity; reference rigidity
C; C_0	orbit length, $C = 2\pi R + \left[\begin{smallmatrix}\text{straight}\\ \text{sections}\end{smallmatrix}\right.$; reference, $C_0 = C(p = p_0)$
E	particle energy
EFB	Effective Field Boundary
f_{rev}, $f_{\mathrm{rf}} = h\, f_{\mathrm{rev}}$	revolution and RF accelerating voltage frequencies
G	gyromagnetic anomaly, $G = 1.792847$ for proton
G; $K = G/B\rho$	quadrupole gradient; focusing strength
h	RF harmonic number
m; m_0; M	mass, $m = \gamma m_0$; rest mass; in units of MeV/c^2
$\mathbf{p}$; p; p_0	momentum vector; its modulus; reference
P_i, P_f	beam polarization, initial, final
q	particle charge
r, R	orbital radius ; average radius, $R = C/2\pi$
s	path variable
v	particle velocity
$V(t)$; $\hat{V}$	oscillating voltage; its peak value
x, x', y, y', l, $\frac{dp}{p}$	horizontal, vertical, longitudinal coordinates in moving frame
α	depending on the context: momentum compaction or trajectory deviation
$\beta = v/c$; β_0; β_{s}	normalized particle velocity; reference; synchronous
β_{u}	betatron functions ($u:\ x, y, Y, Z$)
$\gamma = E/m_0$	Lorentz relativistic factor
δp	momentum offset or Dirac distribution
Δp	momentum offset
ε	wedge angle
ε_u	Courant-Snyder invariant ($u:\ x, r, y, l, Y, Z, s$, etc.)
ϵ_R	strength of a depolarizing resonance
μ_{u}	betatron phase advance, $\mu_{\mathrm{u}} = \int_{\mathrm{period}} ds/\beta_{\mathrm{u}}(s)$ ($u:\ x, y, Y, Z$)
ν_{u}	wave numbers, horizontal, vertical, synchrotron ($u:\ x, y, Y, Z, l$)
ρ, ρ_0	curvature radius; reference
σ	beam matrix
ϕ; ϕ_{s}	particle phase at voltage gap; synchronous phase
ϕ_{u}	betatron phase advance, $\phi_{\mathrm{u}} = \int ds/\beta_{\mathrm{u}}$ ($u:\ x, y, Y, or Z$)
φ	spin angle to the vertical axis

10.1 Introduction

In the very manner that the 1930s-1940s cyclotron, betatron, microtron, weak focusing synchrotron, still in use today, have since essentially not changed in their concepts, design principles, magnet gap profile, today's gap profile, yoke and current coil geometry of combined function alternating-gradient (AG) dipoles remain essentially as patented in 1950 (Fig. 10.1) [1].

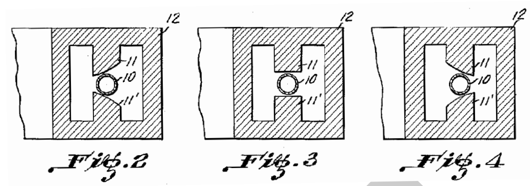

Fig. 10.1 Bending magnet pole profiles for a *focusing system for ions and electrons* [1]. Assuming curvature center to the left, the right (respectively left) profile is defocusing (resp. focusing), the middle profile has zero index

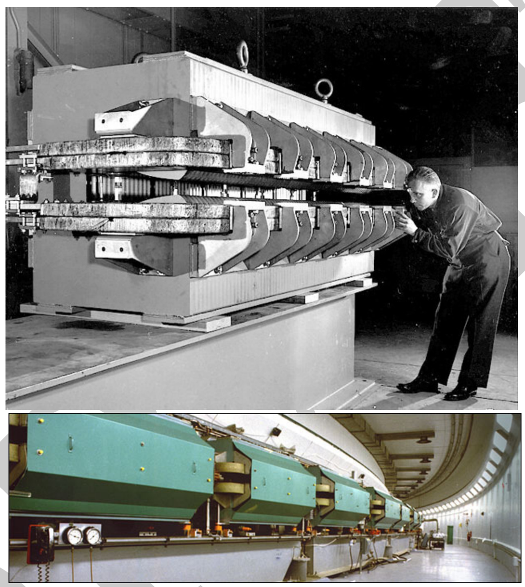

Fig. 10.2 Top: the AGS combined function main magnet - one of 240 steering the beam around the ring, bottom: the 809 m circumference AGS synchrotron [4]. The hyperbolic profile poles are visible on the top photo, partly hidden by the field coils

In 1952, in the context of studies relative to the Cosmotron, strong focusing was devised at the Brookhaven National Laboratory (BNL): *"Strong focusing forces result from the alternation of large positive and negative n-values in successive sectors of the magnetic guide field in a synchrotron. This sequence of alternately converging and diverging magnetic lenses* [...] *leads to significant reductions in oscillation amplitude"* [2]. It led to the construction of the first two high-energy proton AG synchrotrons, in the 30 GeV range, in the late 1950s: the proton-synchrotron (PS) at CERN, and the AGS at BNL (Fig. 10.2), major pieces 60 years later still, of the respective injection chains of the two largest colliders in operation, the LHC and RHIC. Early works at BNL provided theoretical formalism, still at work today, for the analysis of beam dynamics in synchrotrons [3].

Fig. 10.3 A quadrupole magnet at LBL in 1957, used for beam lines at the 184-inch cyclotron. An early specimen here, obviously, being a spin-off of the early 1950s concept of strong focusing [11]

Fig. 10.4 SATURNE II strong focusing 3 GeV synchrotron at Saclay, successor in the late 1970s of Saturne I weak focusing synchrotron (Fig. 9.1). It was the first strong focusing synchrotron to accelerate polarized ion beams

Separated function focusing, whereby beam guiding is ensured by uniform field dipoles while focusing is ensured separately by quadrupoles, followed from the development of the latter (Fig.10.3), a spin-off of the strong index technology [9] (Fig. 10.4).

The dramatic reduction of transverse beam size by strong focusing allows small dipole gaps, thus small magnets: from lowest energies (medical synchrotrons in the 100 MeV range for instance) to the highest ones (particle physics and nuclear physics colliders, hundreds of GeV to multi-TeV range), beams are essentially confined in a centimeter scale transverse space, making a synchrotron a string of dipole magnets containing the beam in a ring vacuum pipe of a few centimeters in diameter (hadrons) or a few millimeters (electrons). The size of the ring is essentially determined by its circumference, proportional to the magnetic rigidity. This revolutionized the race to high energies, from the prior few GeV weak focusing synchrotrons and their huge magnets, to todays 7 TeV at the LHC with magnets transverse size of a few tens of centimeters, and with further plans for 100 TeV rings [5]. It fostered the development of high energy synchrotron light sources around the world, with high brightness synchrotron radiation produced using electron beams in the GeV energy range.

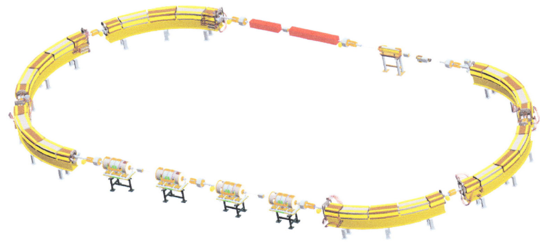

Fig. 10.5 The ion rapid cycling medical synchrotron (iRCMS) [6], an RCS aimed at providing ion beams for the treatment of cancer tumors

AG focusing is still resorted to today, for instance in the hadrontherapy application (Fig. 10.5), light source lattice [7], and other high energy collider design [8], as it has the merit of compactness. On the other hand, the flexibility of separated function optics made it far more popular: it allows to introduce modular functions in complex ring designs such as dispersion suppression sections, low-beta or insertion device sections, long straights, et cetera. Low-emittance, high-brightness light source lattices have complicated focusing further, by introducing longitudinal field gradient bending systems for minimal emittance [10].

Due to the necessary ramping of the field in order to maintain a constant orbit, synchrotron accelerators are pulsed, storage rings in some cases as well, high energy colliders in particular to bring beams to highest store energy. The acceleration is cycled and the accelerating voltage frequency as well in ion accelerators, from injection to top energy. If the ramping uses a constant electromotive force, then (Eq. 9.3)

$$B(t) \approx \frac{t}{\tau} \tag{10.1}$$

$\dot{B} = dB/dt$ does not exceed a few Tesla/second, thus the repetition rate of the acceleration cycle if of the order of a Hertz. If instead the magnet winding is part of a resonant circuit then the field oscillates,

$$B(t) = B_0 + \frac{\hat{B}}{2}(1 - \cos \omega t) \tag{10.2}$$

so that, in the interval of half a voltage repetition period (*i.e.*, $t : 0 \to \pi/\omega$) the field increases from an injection threshold value to a maximum value at highest rigidity, $B(t) : B_0 \to B_0 + \hat{B}$. The latter determines the highest achievable energy: $\hat{E} = pc/\beta = q\hat{B}\rho c/\beta$. The repetition rate with resonant magnet cycling can reach a few tens of Hertz, a technique known as a rapid-cycling synchrotron (RCS). In both cases anyway B imposes its law and the other parameters comprising the acceleration cycle the RF frequency in particular, will follow B(t).

Rapid cycling allows high intensity beams. Instances are the Cornell 12 GeV, 60 Hz, electron AG synchrotron, commissioned in 1967, still in use half a century later as the injector of Cornell 5 GeV synchrotron light source (CHESS); Fermilab 8 GeV, 60 Hz, booster which provides protons for the production of neutrino beams; the 30 GeV 500 kW beam J-PARC facility in Japan. Rapid cycling is also considered in ion-therapy applications, Fig. 10.5.

10.2 Basic Concepts and Formulæ

Alternating gradient focusing is sketched in Fig. 10.6.

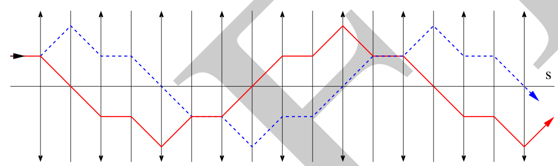

Fig. 10.6 Horizontally focusing lenses (field index $n \gg 0$, the solid red trajectory) are vertically defocusing ($n \ll 0$, the dashed blue trajectory), and vice versa. This imposes alternating gradients in order for a sequence to be globally focusing.

The focusing index value can be estimated from the fields met in these structures: say a maximum B∼1 Tesla in the dipole gap, and as well at pole tip in quadrupoles ∼10 cm off axis. The latter results in $\frac{\Delta B}{\Delta x} \sim 10\,\mathrm{T/m}$, the former in meters to tens of meters dipole curvature radius. All in all,

$$n = \frac{\rho}{B}\frac{\partial B}{\partial x} \sim \frac{10^{0\sim2}_{[\mathrm{m}]}}{1_{[\mathrm{T}]}} \times 10_{[\mathrm{T/m}]} \sim 10^{1\sim3} \quad \gg 1 \tag{10.3}$$

much greater than in a weak focusing structure, characterized by $0 < n < 1$.

10.2.1 Components of the Strong Focusing Optics

Combined function (AG) optics

This is, typically, the BNL AGS and CERN PS optics, using dipoles that ensure both beam guiding and focusing (Fig. 10.2). Separate quadrupole and multipole lenses have later been introduced in these lattices as they provide knobs for the adjustment of optical functions and parameters.

AG optics is still at work in modern designs, as in the iRCMS whose six 60 deg arcs are comprised of a sequence of five focusing and defocusing combined function dipoles [6], Fig. 10.5.

Field

Referring to the normal conducting magnet technology, an hyperbolic pole profile (Fig. 10.1) is an equipotential (a line of constant magnetic potential V) of equation

$$V_{\mathrm{pole}} = A\,xy$$

at the origin of a magnetic field $\mathbf{B} = \mathbf{grad}\,V$, everywhere perpendicular to the equipotential. A combined function dipole with mid-plane geometrical symmetry is defined by materializing two equipotentials, at $\pm V_{\mathrm{pole}}$ (Fig. 10.7). This results in a

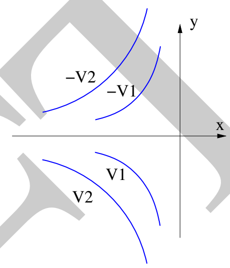

Fig. 10.7 Symmetric materialization of pole profiles, at $\pm V$. Nothing would preclude materializing poles at V_1 and $-V_2$ potentials, with the same resulting field between the poles

vertical field component $B_y = \partial V/\partial y = Ax$, and therefore a radial field index

$$n = \frac{\rho}{B_y}\frac{\partial B_y}{\partial x}\bigg|_{y=0} = \frac{\rho}{B_y}A$$

A is a constant, typically up to $\sim 10\,\mathrm{T/m}$, *cf.* Eq. 10.3. The pole profile opens up either inward (toward the center of curvature, a horizontally focusing dipole, vertically defocusing) or outward (a vertically focusing dipole, horizontally defocusing), Fig. 10.8.

In a bent AG dipole a line of constant field is an arc of a circle; the field guides the reference particle along the arc in the median plane. The mid-plane field can be expressed under the form

$$B_y(r,\theta) = \mathcal{G}(r,\theta)\,B_0\left(1 + n\,\frac{r-r_0}{r_0} + n'\left(\frac{r-r_0}{r_0}\right)^2 + n''\left(\frac{r-r_0}{r_0}\right)^3 + \ \ldots\right) \quad (10.4)$$

with r_0 the reference (normally the orbit) radius. Higher order indices, sextupole n', octupole n'', ..., may be residual effects from fabrication tolerances, magnetic saturation, deformation of yoke with years, etc., or included by design, with significant value.

In a straight AG dipole a line of constant field is a straight line; an instance is the AGS main magnet (Fig. 10.2). Another instance is the Fermilab recycler arcs permanent magnet dipole, which includes quadrupole and sextupole components [13,

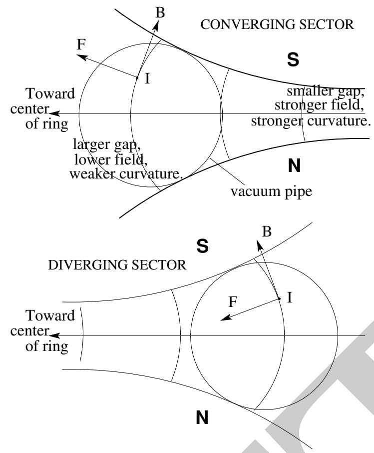

Fig. 10.8 Beam focusing in combined function dipoles. The center of curvature is to the left. The pole profile follows an equipotential $V = Axy$. Top: the pole profile opens up towards the center of curvature → the dipole is horizontally converging (vertically diverging: current I comes out of the page, force **F** results from field **B**). Bottom: pole profile closing toward the center of curvature → the dipole is horizontally diverging, vertically converging

14]. The modeling of the field in a straight combined function dipole can be derived from the scalar potential of Eq. 10.5.

Separated function optics

In a separated function lattice main bends have zero index and ensure beam guiding, whereas quadrupole lenses ensure the essential of the focusing. In smaller rings though, geometrical focusing in bending magnets may be significant (see Sect. 9.2.1.2, Fig. 9.6), wedge angles in addition may be introduced and contribute horizontal and vertical focusing/defocusing (Fig. 9.9).

Higher order multipole lenses are used for the compensation of adverse effects: coupling, aberrations, space charge, impedance, etc., and for beam manipulations: coupling, resonant extraction, etc.

The field in a multipole of order n ($n = 1, 2, 3,$ etc.: dipole, quadrupole, sextupole, etc.) derives, via $\mathbf{B} = \mathbf{grad}V$, from the Laplace potential [16]

$$V_n = (n!)^2 \left\{ \sum_{\mathrm{q}=0}^{\infty} (-)^q \alpha_{\mathrm{n},0}^{(2q)}(s) \frac{(x^2+y^2)^q}{4^q q!(n+q)!} \right\} \left\{ \frac{x^{n-m} y^m}{m!(n-m)!} \sin m\frac{\pi}{2} \right\} \qquad (10.5)$$

wherein $\alpha_{\mathrm{n},0}^{(2q)}(s) = d^{2q}\alpha_{\mathrm{n},0}(s)/ds^{2q}$ accounts for the s-dependence of the field. Technologies for multipoles and combined multipoles include pole profiling, permanent magnets [13, 18], superconducting $\cos\theta$ windings as in RHIC and LHC colliders, and variants of all sorts.

In a hard-edge field model the $\sum_{\mathrm{q}=0}^{\infty}$ factor in Eq. 10.5 is reduce to the $q = 0$ term, with the following outcomes.

Quadrupole [1]

The equipotential (the pole profile) is an equilateral hyperbola, of equation Gxy =constant in an upright quadrupole (left), and $G(x^2-y^2)$ =constant in a $\pi/4$ skewed quadrupole (right). The resulting field writes

$$B_x = \frac{\partial V}{\partial x} = Gy \qquad B_y = \frac{\partial V}{\partial y} = Gx$$

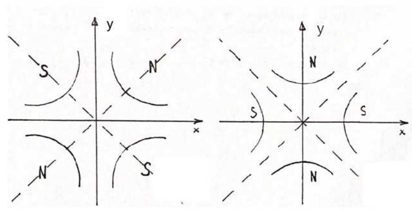

$$B_x = Gx \qquad B_y = -Gy$$

Upright quadrupoles are used for focusing, skew quadrupoles are used to compensate, or introduce, transverse coupling. Their focusing strength

$$K = \frac{1}{L}\frac{\int G(s)\,ds}{p/q}$$

is momentum-dependent.

Sextupole

The equipotential satisfies $H(3x^2y - y^3)$ =constant in an upright sextupole (left), $H(x^3 - 3xy^2)$ =constant in a $\pi/6$ skewed sextupole (right), with resulting field

$$B_x = 2Hxy \qquad B_y = H(x^2 - y^2)$$

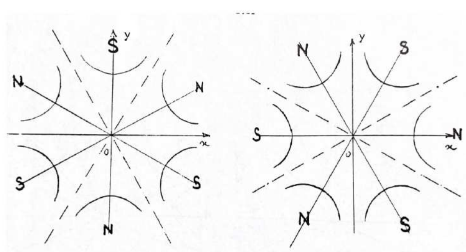

$$B_x = H(x^2 - y^2) \qquad B_y = -2Hxy$$

Upright sextupoles introduce a vertical field component $B_y \propto x^2$, they are used to correct optical aberrations, to modify the momentum dependence of the wave numbers ν_x, ν_y, and in beam manipulations such as resonant extraction. Skew

[1] This introduction to the methods of strong focusing optics owes much to Ref. [19].

sextupoles introduce a radial field component $B_x \propto y^2$, they are used to correct optical aberrations.

Octupole

The equipotential pole profile satisfies $O(x^3y - xy^3)$ =constant in an upright octupole (left), $O(x^4 - 6x^2y^2 + y^4)$ =constant in a $\pi/8$ skewed octupole (right), yielding the field

$$B_x = O(3x^2y - y^3) \qquad B_y = O(x^3 - 3xy^2)$$

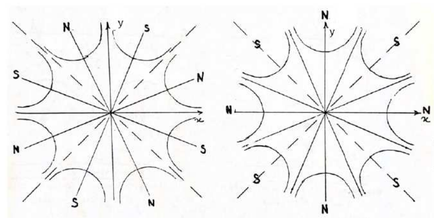

$$B_x = O(x^3 - 3xy^2) \qquad B_y = -O(3x^2y - y^3)$$

Upright octupoles are used to introduce a vertical field component $B_y \propto x^3$; skew octupoles introduce a vertical field component $B_y \propto y^3$. Octupoles are used to correct aberrations, or to modify the amplitude dependence of wave numbers.

10.2.2 Transverse motion

The transverse motion of a particle in the periodic lattice of a cyclic accelerator satisfies Hill's equations

$$\frac{d^2x}{ds^2} + K_x(s)x = \frac{1}{\rho_0}\frac{\Delta p}{p_0}, \qquad \frac{d^2y}{ds^2} + K_y(s)y = 0 \tag{10.6}$$

where $K_x(s)$, $K_y(s)$ have the periodicity of the lattice, and depend locally on the nature of the optical elements:

$$\begin{aligned}
&- \text{dipole :} && \begin{cases} K_x = \dfrac{1-n}{\rho_0^2} \\ K_y = \dfrac{n}{\rho_0^2} \end{cases} \qquad \left(n = -\frac{\rho_0}{B_0}\frac{\partial B_y}{\partial x}\right) \\
&- \text{a wedge at } s = s_w : && \Big\{ K_{\substack{x\\y}} = \pm\frac{\tan\varepsilon}{\rho_0}\delta(s - s_w) \quad \left(\text{with } \varepsilon \lesseqgtr 0 \text{ for } \begin{matrix}\text{focusing}\\ \text{defocusing}\end{matrix}\right) \\
&- \text{quadrupole} && \left(\text{gradient } G = \frac{\text{field at pole tip}}{\text{radius at pole tip}}\right) : K_{\substack{x\\y}} = \frac{\pm G}{B\rho};\ \frac{1}{\rho_0} = 0 \\
&- \text{drift space :} && K_x = K_y = 0;\ \frac{1}{\rho_0} = 0
\end{aligned} \tag{10.7}$$

By contrast with the betatron and weak focusing technologies, strong focusing with its independent focusing ($G > 0$) and defocusing ($G < 0$) families allows separate adjustment of the horizontal and vertical focusing strengths, and wave numbers as a consequence.

The on-momentum ($p = p_0$) closed orbit coincides with the reference axis of the optical structure. The betatron motion for an on-momentum particle satisfies Eq. 10.6 with $\Delta p = 0$. Solving the latter (see Sect. 9.2) requires introducing two independent solutions $u_{\frac{1}{2}}(s)$ (Eq. 9.12), the linear combination of which yields the pseudo harmonic motion (Eq. 9.15)

$$\left| \begin{array}{l} u(s) = \sqrt{\beta_u(s)\varepsilon_u/\pi}\,\cos\left(\int \frac{ds}{\beta_u(s)} + \varphi_u\right) \\ u'(s) = -\sqrt{\frac{\varepsilon_u/\pi}{\beta_u(s)}}\,\sin\left(\int \frac{ds}{\beta_u(s)} + \varphi_u\right) + \alpha(s)\,\cos\left(\int \frac{ds}{\beta_u(s)} + \varphi_u\right) \end{array} \right. \tag{10.8}$$

The motion satisfies the Courant-Snyder invariant, namely (Fig. 9.10)

$$\gamma_u(s)u^2 + 2\alpha_u(s)uu' + \beta_u(s)u'^2 = \frac{\varepsilon_u}{\pi} \tag{10.9}$$

i.e., the surface of the phase space ellipse is a constant of the motion. Its form and orientation change along the period as a consequence of the strong modulation of the betatron functions (Fig. 10.9), far more than in a weak focusing lattice where $\alpha_u(s) \approx 0$ and $\beta_u(s) \approx$constant.

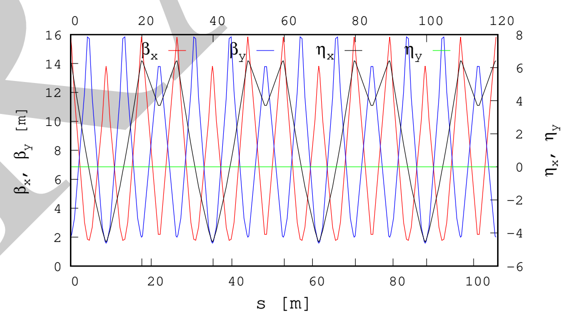

Fig. 10.9 Optical functions in SATURNE II synchrotron, a 4-period FODO cell lattice (see exercise 10.1)

Beam envelopes are given by the extrema,

$$\hat{x}_{\mathrm{env}}(s) = \pm\sqrt{\beta_x(s)\frac{\varepsilon_x}{\pi}}, \qquad \hat{y}_{\mathrm{env}}(s) = \pm\sqrt{\beta_y(s)\frac{\varepsilon_y}{\pi}} \tag{10.10}$$

Phase space motion

Write the two independent solutions $u_{\frac{1}{2}}(s)$ (Eq. 9.12) under the form

$$u_1(s) = \underbrace{F(s)}_{\text{S-periodic}} \times \underbrace{e^{i\mu\frac{s}{S}}}_{\frac{2\pi S}{\mu}\text{-periodic}} \quad \text{and} \quad u_2(s) = u_1^*(s) = F^*(s)\, e^{-i\mu\frac{s}{S}} \tag{10.11}$$

wherein $F(s) = \sqrt{\beta_u(s)}\, e^{i\left(\int_0^s \frac{ds}{\beta_u(s)} - \mu\frac{s}{S}\right)}$. Introduce $\psi_u(s) = \int_0^s \frac{ds}{\beta_u(s)} - \mu\frac{s}{S}$ so that $F(s) = \sqrt{\beta_u(s)}\, e^{i\psi_u(s)}$, Eq. 10.8 thus takes the form

$$\left|\begin{aligned} u(s) &= \overbrace{\sqrt{\beta_u(s)\varepsilon_u/\pi}}^{S\text{-periodic}}\ \overbrace{\cos\left[\nu\frac{s}{R} + \underbrace{\psi_u(s)}_{\text{S-per.}} + \varphi_u\right]}^{\frac{2\pi S}{\mu}\text{-periodic}} \\ u'(s) &= -\sqrt{\frac{\varepsilon_u/\pi}{\beta_u(s)}}\ \sin\left[\nu\frac{s}{R} + \psi_u(s) + \varphi_u\right] + \alpha(s)\ \cos\left[\nu\frac{s}{R} + \psi_u(s) + \varphi_u\right] \end{aligned}\right. \tag{10.12}$$

wherein $\nu = \dfrac{N\mu}{2\pi}$. Thus, as the betatron function $\beta_u(s)$ and phase $\psi_u(s)$ are S-periodic, the turn-by-turn motion observed at a given azimuth s (*i.e.*, $u(s)$, $u(s+\mathcal{S})$, $u(s+2\mathcal{S})$, ...) is sinusoidal and its frequency is $\nu = N\mu/2\pi$. Successive particle positions $(u(s), u'(s))$ in phase space lie on the Courant-Snyder invariant (Eq. 10.9).

The wave numbers ν_x and ν_y can be adjusted independently in a separated function lattice, by means of two independent quadrupole families. The working point (ν_x, ν_y) fully characterizes the first order optical setting of the ring.

Off-momentum motion

The motion of an off-momentum particle satisfies the inhomogeneous Hill's horizontal differential Eq. 10.6. The chromatic closed orbit

$$x_{\mathrm{ch}}(s) = D_x(s)\frac{\delta p}{p} \tag{10.13}$$

is a particular solution of the equation, its periodicity is that of the cell.

By contrast with the weak focusing configuration, where the on-momentum closed orbit and chromatic closed orbits are parallel (Eq. 9.26: D_x=constant, independent of s), chromatic closed orbits in a strong focusing optical structure are distorted (Fig. 10.9), their excursion depends on the distribution along the cell of (i) the dispersive elements which are the dipoles, and (ii) the focusing.

The horizontal motion of an off-momentum particle is a superposition of the particular solution (Eq. 10.13) and of the betatron motion, solution of the homogeneous Hill's equation (Eq. 10.6 with $\delta p/p = 0$), namely

$$x(s) = x_\beta(s) + x_{\mathrm{ch}}(s) = \sqrt{\beta_x(s)\frac{\varepsilon_x}{\pi}}\,\cos\left(\int \frac{ds}{\beta_x} + \varphi_x\right) + D_x(s)\frac{\Delta p}{p_0} \tag{10.14}$$

whereas the vertical motion is unchanged (Eq. 10.12 taken for $u(s) \equiv y(s)$).

Adiabatic damping of the betatron oscillations

The mechanism is addressed in Sect. 10.2.2 (and its solution in more detail in Sect. 11.2.3). In the case of an adiabatic change of momentum $p = \beta\gamma m_0 c$ (a slow change compared to the betatron motion oscillation frequency) the transverse motion damping satisfies

$$p\,\varepsilon_u = \text{constant}, \quad \text{or} \quad \beta\gamma\varepsilon_u = \text{constant} \tag{10.15}$$

Coordinates damping satisfies (Eq. 11.21 with R =constant, constant orbit radius)

$$x, y \propto 1/\sqrt{p}, \qquad x', y' \propto 1/\sqrt{p} \tag{10.16}$$

10.2.3 Resonances

Consider the excitation of transverse beam motion by a generator of frequency Ω located at some azimuth along the ring [19]. The action of the excitation $S \times \sin\Omega t$ on the oscillating motion $u(t)$ can be written under the form

$$\frac{d^2u}{dt^2} + \omega^2 u = S\sin\Omega t \tag{10.17}$$

Assume harmonic motion for simplicity (as in a weak focusing lattice). Take S constant, the solution (superposition of the solution of the homogeneous differential equation and of a particular solution of the inhomogeneous differential equation) writes

$$u(t) = U\cos(\omega t + \varphi_u) + \frac{S}{\omega^2 - \Omega^2}\sin\Omega t \tag{10.18}$$

If betatron motion and excitation are in synchronism, *i.e.* on the resonance, $\omega = \Omega$, a particular solution of Eq. 10.17 is

$$u_r(t) = -\frac{S\,t}{2\Omega}\cos\Omega t$$

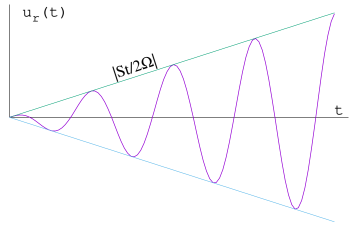

the amplitude of the oscillatory motion grows rapidly with time, at a rate $|St/2\Omega|$.

Assume S periodic instead, take its Fourier expansion $S(t) = \sum_{p=0}^{\infty} a_p \cos(p\omega' t + \varphi_p)$, the equation of motion thus writes

$$\frac{d^2u}{dt^2} + \omega^2 u = \sum_{p=0}^{\infty} a_p \cos(p\omega' t + \varphi_p)\ \sin\Omega t =$$

$$\sum_{p=0}^{\infty} \frac{a_p}{2}\Big[\sin[(\Omega - p\omega')t + \varphi_p] + \sin[(\Omega + p\omega')t + \varphi_p]\Big]$$

Resonance may occur at oscillator frequencies $\omega = \Omega \pm p\omega'$, their strength depends on the amplitude a_p of the excitation harmonics. If the generator is located at one point in the ring, it excites all harmonics.

Sextupole and octupole resonances

The horizontal motion in the presence of sextupoles ($B_y(\theta)|_{y=0} = S(\theta)x^2$, see *Sextupole*, above) satisfies

$$\frac{d^2x}{d\theta^2} + \nu_x^2 x = S(\theta)x^2 \tag{10.19}$$

Assume weak perturbation of the motion, so that $x(\theta) \approx \hat{x}\cos(\nu_x\theta + \varphi_x)$, the solution for unperturbed motion, and $S(\theta)$ 2π-periodic. Substitute its Fourier series expansion $S(\theta) = \sum_{p=0}^{\infty} a_p \cos(p\omega'\theta + \varphi_p)$ in Eq. 10.19, develop to get

$$\frac{d^2x}{d\theta^2} + \nu_x^2 x = \frac{\hat{x}^2}{2}\sum_{\mathrm{p=0}}^{\infty} a_p \Big[\cos(p\theta + \varphi_p) +$$

$$\cos[(p - 2\nu_x)\theta + \varphi_p - 2\varphi_x]\ +\ \cos[(p + 2\nu_x)\theta + \varphi_p + 2\varphi_x]\Big]$$

Thus resonance may occur at betatron frequency families $\nu_x = \pm p$, $\nu_x = \pm(p - 2\nu_x)$, and $\nu_x = \pm(p + 2\nu_x)$, *i.e.*,

$$\left[\begin{array}{l}\nu_x = \text{integer}\\ 3\nu_x = \text{integer}\end{array}\right.$$

In the case of a single sextupole in the ring, all the harmonics p are excited with the same amplitude a_p.

An octupole perturbation introduces a field component $B_y(\theta)|_{y=0} = O(\theta)x^3$ (see *Octupole*, above) in the optical lattice. In a similar way, assume weak perturbation so that $x(\theta) \approx \hat{x}\cos(\nu_x\theta + \varphi_x)$, and to $O(\theta)$ substitute its Fourier expansion. This yields the resonant betatron frequencies

$$\begin{cases} \nu_x = \text{integer} \\ 2\nu_x = \text{integer} \\ 4\nu_x = \text{integer} \end{cases}$$

Resonances in a general manner occur at betatron frequencies satisfying

$$m\nu_x + n\nu_y = \text{integer}$$

with the property that

$$\frac{\varepsilon_x}{m} - \frac{\varepsilon_y}{n} = \text{constant}, \qquad \text{an invariant of the motion}$$

with the following consequences:

- if m and n have opposite signs the resonance causes energy exchange between the horizontal and vertical motions: $\frac{\varepsilon_x}{|m|} + \frac{\varepsilon_y}{|n|} = \text{constant}$, an increase of ε_x correlates with a decrease of ε_y and vice-versa; in the presence of linear coupling for instance, $\nu_x - \nu_y = \text{integer}$, $\varepsilon_x + \varepsilon_y = \text{constant}$. An increase in motion amplitude anyway may cause particle loss, an issue in cyclotrons for instance where the Walkinshaw resonance $\nu_x = 2\nu_y$ causes vertical beam loss due to the increase of ε_y;
- if m and n have the same sign the resonance induces motion instability: $\frac{\varepsilon_x}{m} - \frac{\varepsilon_y}{n} = \text{constant}$, ε_x and ε_y may both increase with no limit.

Resonant Extraction

Resonant extraction is based on the effect of a non-linear force on a dynamical system. A linear regime, under the effect of linear forces, saisfies Eq. 10.6, if $x(s)$ is a stable solution, so is $\lambda x(s)$ (λ a proportionality constant). Introducing a non-linear force modifies the equation of motion, into for instance

- $\frac{d^2x}{ds^2} + K_x(s)x = S(s)x^2$: sextupole perturbation,
- $\frac{d^2x}{ds^2} + K_x(s)x = O(s)x^3$: octupole perturbation,

If $x(s)$ is a stable solution, it may no longer be the case for $\lambda x(s)$. If $x(s)$ is small enough the motion, subject to linear and non-linar forces, is quasi-linear and stable. However, increasing the motion amplitude will at some point result in unstable motion. In the (x, x') phase space, the stable regime is bounded by a separatrix. Outside the latter the motion is essentially unstable, or liable to reach amplitudes far beyond transverse acceptance of the accelerator (Fig. 10.10),

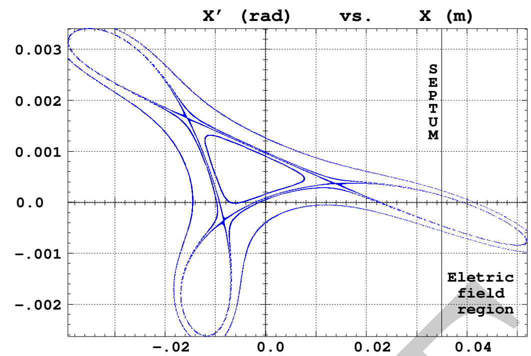

Fig. 10.10 Horizontal motion near a 3rd integer resonance. Within the separatrix the motion regime varies with $\hat{x}$ but it is stable. Outside the separatrix the motion reaches prohibitive amplitudes. A septum allows an electrostatic field (to its right, here) which kicks into an extraction optical channel those particles reaching that phase space region in the course of their motion outside the separatrix

10.2.4 Synchrotron Motion

Particle motion in the longitudinal phase space (phase, momentum) is determined by the lattice and by the acceleration parameters, introduced in Sect. 9.2.2. They include the RF

- frequency $f_{\mathrm{rf}} = h f_{\mathrm{rev}}$,
- synchronous phase ϕ_s, which increases by $2\pi h$ per turn (Fig. 9.15),
- voltage $V(t) = \hat{V} \sin \omega_{\mathrm{rf}} t = \hat{V} \sin \phi_s$

The energy gain per turn at the cavity is

$$\Delta W = 2\pi R\, q\rho\dot{B} = q\hat{V} \sin \phi_s$$

ΔW is imposed by the field law in order to ensure that at all time the synchronous particle momentum satisfies

$$p_s(t) = qB(t)\rho$$

Phase stability

The angular frequency of the phase space motion is

$$\Omega_s = \omega_{\mathrm{rev}} \sqrt{\frac{|\eta| hq\hat{V} \cos \phi_s}{2\pi E_s}}$$

In this expression,

- $E_s = m\gamma$ is the synchronous energy,
- $\omega_{\mathrm{rev}} = \frac{1}{T_{\mathrm{rev}}} = \frac{qB\rho}{2\pi Rm}$ the revolution angular frequency,
- $\eta = \frac{d\omega_{\mathrm{rev}}}{\omega_{\mathrm{rev}}} = \frac{1}{\gamma^2} - \alpha$ the phase slip factor (Eq. 9.33),
- $\alpha = \gamma_{\mathrm{tr}}^{-2} = \frac{\Delta C/C}{\Delta p/p_0}$ the momentum compaction,
- γ_{tr} which determines the stable synchronous phase region, $\phi_s \in [0, \pi/2]$ or $\phi_s \in [\pi/2, \pi]$.

In a soft betatron focusing lattice (weak focusing, or AG lattice), $\alpha \approx 1/\nu_x^2$ so that $\eta = \frac{d\omega_{\rm rev}}{\omega_{\rm rev}} = \frac{1}{\gamma^2} - \frac{1}{\nu_x^2}$, thus

$$\gamma_{\rm tr} \approx \nu_x$$

Some instances: SATURNE I (a weak focusing lattice, see Chap. 9 and simulations therein) operated above transiton as $\nu_x \approx 0.6$; SATURNE II lattice had a negative α, $\eta = \frac{1}{\gamma^2} - \alpha$ cannot cancel in that case, $\gamma_{\rm tr}$ is pure imaginary; the working point of the AGS at BNL is $\nu_x \approx 8.7$, $\gamma_{\rm tr} = 8.4 \approx \nu_x$ is crossed as proton beams are accelerated from $\gamma \approx 3$ to $\gamma \approx 25$, referring to Fig. 9.15 the RF phase is quickly moved from region A to region B of the accelerating voltage oscillation.

The bucket height is the momentum acceptance and given by

$$\pm\frac{\Delta p}{p} = \pm\frac{1}{\beta}\sqrt{\frac{q\hat{V}}{\pi h\eta E_s}\,[-(\pi - 2\phi_s)\sin\phi_s + 2\cos\phi_s]} \tag{10.20}$$

The maximum extent in phase for small amplitude oscillations satisfies

$$\pm\Delta\phi_{\rm max} = \frac{h\eta E_s}{p_s R_s \Omega_s} \times max\left(\frac{\Delta E}{E_s}\right) \tag{10.21}$$

****** separatrix **********

The motion of a particle with energy offset $\delta E = E - E_s$ satisfies the longitudinal invariants

$$\epsilon_l = \frac{\alpha E_s}{2\Omega_s}\left[\left(\frac{\delta E}{E_s}\right)^2 + \frac{1}{\Omega_s^2}\left(\frac{d}{dt}\frac{\delta E}{E_s}\right)^2\right] \tag{10.22}$$

$$(\widehat{\delta E})^2 = (\delta E)^2 + \frac{1}{\Omega_s^2}\left(\frac{d\delta E}{dt}\right)^2 \tag{10.23}$$

Introducing the squared *rms* relative synchrotron amplitude $\sigma^2_{\widehat{\delta E}/E} \equiv (\widehat{\delta E}/E_s)^2$ this yields in addition

$$\epsilon_l = \frac{\alpha E_s}{2\,\Omega_s}\,\sigma^2_{\widehat{\delta E}/E} \tag{10.24}$$

10.2.5 Depolarizing resonances

By contrast with weak focusing optics where depolarizing resonances are weak because horizontal field components are weak (Sect. 9.2.3), the use of strong focusing field gradients in the combined function magnets and/or focusing lenses of strong focusing optics results in strong radial field components and therefore strong depolarizing resonances.

Spin precession and resonant spin motion in the magnetic components of a cyclic accelerator have been introduced in Sects. 4.2.5, 5.2.5. The general conditions for depolarizing resonance to occur have been introduced in Sect. 9.2.3. In a strong focusing synchrotron they essentially result from the radial field components in the focusing magnets and their strength is determined by the lattice optics, as follows.

Strength of imperfection resonances

Imperfection, or integer, depolarizing resonances are driven by a non-vanishing vertical closed orbit $y_{\text{co}}(\theta)$ which causes spins to experience periodic radial fields in focusing magnets, dipoles in combined function lattices and quadrupoles in separated function lattices, namely,

$$B_x(\theta) = G\,y(\theta) = K(\theta) \times B_0\rho_0 \times y_{\text{co}}(\theta) \tag{10.25}$$

with θ the orbital angle, $B_0\rho_0$ the lattice rigidity and $y_{\text{co}}(\theta)$ the closed orbit excursion. Resonance occurs if the spin undergoes an integer number of precessions over a turn (it then undergoes 1-turn-periodic torques), so that spin tilts at field perturbations along the closed orbit add up coherently. Thus resonances occur at integer values

$$G\gamma_n = n$$

A Fourier development of these perturbative fields yields the strength of the $G\gamma_n$ harmonic [24, Sect. 2.3.5.1]

$$\epsilon_n^{\text{imp}} = (1 + G\gamma)\frac{R}{2\pi} \oint K(\theta)\ y_{\text{co}}(\theta)\, e^{-jG\gamma(\theta-\alpha)}\, e^{jn\theta}\, d\theta$$

In the thin-lens approximation, near the resonance where $G\gamma - n \to 0$, this simplifies into a series over the quadrupole fields,

$$\epsilon_n^{\text{imp}} = \frac{1+G\gamma_n}{2\pi} \sum_{\text{Qpoles}} [\cos G\gamma_n\,\alpha_i + \sin G\gamma_n\,\alpha_i]\,(KL)_i\ \ y_{\text{co}}(\theta_i) \tag{10.26}$$

with θ_i the quadrupole location, $(KL)_i$ the integrated strength (slice the dipoles as necessary in an AG lattice for this series to converge) and α_i the cumulated orbit deviation.

Orbit harmonics near the betatron tune ($n = G\gamma_n \approx \nu_y$) excite strong resonances. Imperfection resonance strength is further amplified in P-superperiodic rings, with m-cell superperiods, if the betatron tune $\nu_y \approx \text{integer} \times m \times P$ [25, Chap.3-I].

Strength of intrinsic resonances

Intrinsic depolarizing resonances are driven by betatron motion, which causes spins to experience strong radial field components in quadrupoles, namely

$$B_x(\theta) = G\,y(\theta) = K(\theta) \times B_0\rho_0 \times y_\beta(\theta) \tag{10.27}$$

The effect of resonances on spin depends upon betatron amplitude and phase, their effect on beam polarization depends on beam emittance. Longitudinal fields from dipole ends are usually weak by comparison and ignored. The location of intrinsic resonances depends on betatron tune, it is given in an M-periodic structure by

$$G\gamma_n = nM \pm \nu_y$$

A Fourier development of the perturbative fields yields the two families of strengths [24, Sect. 2.3.5.2]

$$\epsilon_n^{\mathrm{intr}\pm} = \frac{\lambda_x \rho_0}{4\pi} \int_0^{2\pi} K(\theta) \sqrt{\beta_y(\theta)\frac{\varepsilon_y}{\pi}}\, e^{\pm j \left(\int_0^{s(\theta)} \frac{ds}{\beta_y} - \nu_y \theta\right)}\, e^{-jG\gamma(\theta - \alpha(\theta))}\, e^{jn\theta} d\theta$$

In the thin-lens approximation, near the resonance where $G\gamma \pm \nu_y - n \to 0$, this simplifies into a series over the quadrupole fields,

$$\begin{Bmatrix} \mathcal{R}e(\epsilon_n^{\mathrm{intr}\pm}) + \\ j\,\mathcal{I}m(\epsilon_n^{\mathrm{intr}\pm}) \end{Bmatrix} = \frac{1 + G\gamma_n}{4\pi} \sum_{\mathrm{Qpoles}} \begin{Bmatrix} \cos(G\gamma_n \alpha_i \pm \varphi_i) + \\ j\, \sin(G\gamma_n \alpha_i \pm \varphi_i) \end{Bmatrix} (KL)_i \sqrt{\beta_{y,i}\frac{\varepsilon_y}{\pi}} \quad (10.28)$$

10.3 Exercises

In complement to the present exercises, an extensive tutorial on depolarizing resonances in a strong focusing synchrotron, considering proton, helion, or electron beams, using the lattice of the AGS Booster at BNL, can be found in Ref. [24, Chap. 14]. The simulations include the use of tune-jump quadrupoles, a solenoid, Siberian snakes, spin rotators in an electron ring and their effect on polarization life time.

10.1 Construct SATURNE II synchrotron. Spin Dynamics With Snakes
Solution: page 361

Over the years 1978-1997 the 3 GeV synchrotron SATURNE II at Saclay (Figs. 10.4, 10.11) delivered polarized proton beams, and polarized deuteron and ^{6}Li beams up to 1.1 GeV/nucleon, for intermediate energy nuclear physics research, including meson production [20, 21]. The separated function synchrotron was designed *ab initio* for the acceleration of polarized beams [23], and the first strong focusing synchrotron to do so - ZGS, first to accelerate polarized beams, protons and deuterons, was a weak focusing synchrotron (see Chap. 9).

SATUNE II is a FODO lattice with missing dipole. Its parameters are given in Tab. 10.1.

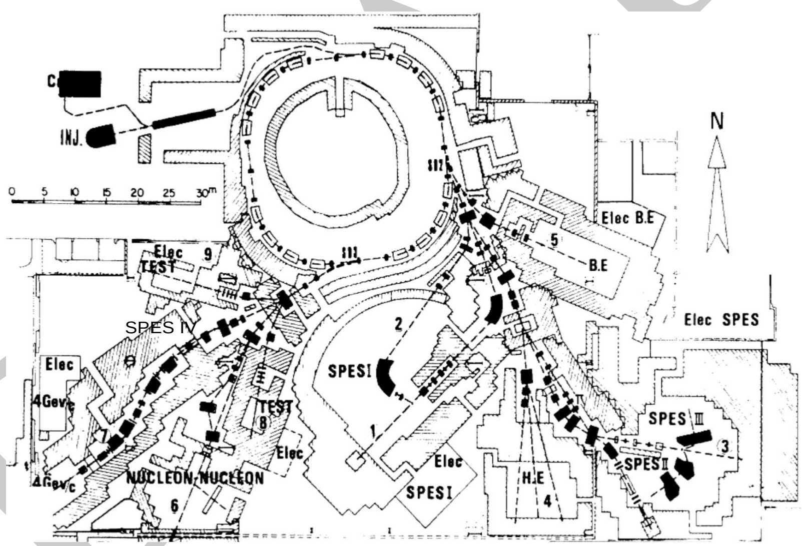

Fig. 10.11 SATURNE II synchrotron and its experimental areas [26], including mass spectrometers SPES I to SPES IV, a typical 1960-80s nuclear physics accelerator facility. Polarized ion sources are on the top left, followed by a 20 MeV linac

(a) Simulate the main dipole using BEND. Dipole fringe fields matter in this small ring, take them into account assuming $\lambda = 8$ cm extent and the following Enge

Table 10.1 Parameters of SATURNE II separated function FODO lattice. ρ_0 denotes the reference bending radius in the main dipole; the reference orbit, wave numbers, etc., are taken along that radius

Orbit length, C	m	105.5556
Average radius, $R = C/2\pi$	m	16.8
Straight sections, length:		
- short	m	0.716256
- long	m	3.92148
Dipole:		
- bend angle, α	deg	$\pi/8$
- magnetic length, $\rho\alpha$	m	2.489
- magnetic radius, ρ	m	6.3381
- wedge angle, ε	deg	2.45
Quadrupole:		
- gradient	T/m	0.5 - 10.56
- magnetic length F/D	m	0.46723 / 0.486273
Wave numbers, ν_x; ν_y		3.64; 3.60
Chromaticities, ξ_x; ξ_y		negative, a few units
Momentum compaction α		0.015
Injection energy (proton)	MeV	20
Top energy	GeV	3
$\dot{B}$	T/s	4.2
Synchronous energy gain	keV/turn	1.160
RF harmonic		2

coefficient values (Eq. 15.13, Sect. 15.2.6):

$$C_0 = 0.2401,\ C_1 = 1.8639,\ C_2 = -0.5572,\ C_3 = 0.3904,\ C_4 = C_5 = 0$$

Produce a graph of the field across the dipole along the reference orbit, in the median plane and at 5 cm vertical distance (CONSTY keyword can be used to force the particle on a constant radius, constant vertical offset trajectory). Produce the transport matrix of the dipole, check against theory. Compare with the matrix of the hard edge model.

Simulate the F and D quadrupoles, using respectively QUADRUPOLE and MULTIPOL. Compare matrices with theory.

Construct the cell. Produce machine parameters (tunes, chromaticities), check against data, Tab. 10.1.

Construct the 4-cell ring. Produce a graph of the optical functions.

(b) Accelerate a bunch with Gaussian densities comprised of a few tens of particles (it can be defined using MCOBJET), from injection to top energy; use harmonic 3 RF frequency, and (unrealistic, for a reduced number of turns) peak RF voltage $\hat{V} = 1$ MV.

Produce a graph of the three phase spaces. Check the transverse betatron damping.

(c) Determine the momentum acceptance of the ring. Produce a graph of the longitudinal phase space separatrix, in the following two cases: stationary bucket and accelerated bucket. Take $\hat{V} = 100$ kV and in the latter case a synchronous phase of 20 deg.

10.2 Injection, extraction

Solution: page 367

(a) Simulate multiturn injection in the ring. Take the injection point at the center of a long straight section.

(b) Simulate resonant extraction from the ring, on $\nu_x = 11/3$. Take the extraction point at the center of a long straight section.

10.3 Depolarizing Resonances In SATURNE II

Solution: page 367

The input data file to simulate the ring is given in Tab. 17.73, an outcome of exercise 10.1.

(a) Calculate the strength of the intrinsic depolarizing resonances (systematic and non-systematic) over 0.5-3 GeV, using Eq. 10.28.

(b) Ggamma=7-ν_y was found to be a potentially harmful depolarizing resonance - unexpectedly as this is not a systematic resonance. Produce a crossing of that resonance, for a 100-particle bunch. Get its strength from this simulation, compare with (a).

(c) Multiple resonance xing - ref to Phys. Rev. article ***

10.4 Cornell electron RCS. Radiative Energy Loss

Short intro .... energy loss by synchrotron radiation [27]

Tab.: RCS parameter list

(a) Cornell RCS parameters are given in Tab. **??**. Construct the ring, produce its optical parameters. Produce a graph of the optical functions.

(b) Raytrace a few tens of particles over 3000 turns in Cornell RCS, from *** to *** GeV. Assume emittances epsilx=, epsily=, Gaussian densities, initial *rms* $\delta p/p = 10^{-4}$. Produce a graph of the three phase spaces. produce graphs of horizontal and vertical transverse excursions versus turn number.

(c) Re-do (b) with synchrotron radiation energy loss.

(d) Produce the average beam polarization obtained in (c).

(c) Multiple resonance crossing.

References

1. Christofilos, Nicholas: Focussing system for ions and electrons. US Patent Office Application filed March 10, 1950, Serial No. 148,920.
https://patentimages.storage.googleapis.com/fa/bb/52/0ce28e28b492a6/US2736799.pdf
2. Courant, Ernest D., Livingston, M. Stanley, and Snyder, Hartland S.: The Strong-Focusing Synchroton - A New High Energy Accelerator. Phys. Rev. 88, 1190 - December 1952
3. Courant, E.D., and Snyder, H.S.: Theory of the Alternating-Gradient Synchrotron. Annals of Physics, No. 3 (1958), 1âĂŞ48
4. Credit: Brookhaven National Laboratory.
https://www.flickr.com/photos/brookhavenlab/8495311598/in/album-72157611796003039/
5. Agapov, I., et al.: Future Circular Lepton Collider FCC-ee: Overview and Status. Submitted on 15 Mar 2022; arXiv:2203.08310 [physics.acc-ph].
https://doi.org/10.48550/arXiv.2203.08310
6. Méot, F., et al.: Progress on the optics modeling of BMIâĂŹs ion rapid-cycling medical synchrotron at BNL. THPMP050, 10th Int. Particle Accelerator Conf. IPAC2019, Melbourne, Australia. https://accelconf.web.cern.ch/ipac2019/papers/thpmp050.pdf
Copyrights under license CC-BY-3.0, https://creativecommons.org/licenses/by/3.0; no change to the material
7. Nishimori, N.: A new compact 3 GeV light source in Japan. 13th Int. Particle Acc. Conf. IPAC2022, Bangkok, Thailand.
https://accelconf.web.cern.ch/ipac2022/papers/thixsp1.pdf
8. Méot, F.: eRHIC ERL modeling in Zgoubi. BNL-111832-2016-TECH; EIC/49;BNL-111832-2016-IR.
https://technotes.bnl.gov/PDF?publicationId=38865
9. Radial Focusing in the Linear Accelerator. Phys. Rev. Vol. 88, Num. 5, Dec. 1, 1952
10. BenabderrahmaneâĂă, C.: Status of the ESRF-EBS magnets. WEPMK009, 9th International Particle Accelerator Conference, IPAC2018, Vancouver, BC, Canada.
https://accelconf.web.cern.ch/ipac2018/papers/wepmk009.pdf
11. Credit: Lawrence Berkeley National Laboratory. The Regents of the University of California, Lawrence Berkeley National Laboratory."
12. SATURNE II photo: credit CEA Saclay. Archives historiques du CEA. Copyright CEA/Service de documentation
13. Jackson, G., Editor: Fermilab recycler ring technical design report. Rev. 1.1. FERMILAB-TM-1981 (July 1996).
http://inspirehep.net/record/424541/files/fermilab-tm-1981.PDF
14. Méot, F.: On the Effects of Fringe Fields in the Recycler Ring. FERMILAB-TM-2016 (Aug. 1997).
http://inspirehep.net/record/448603/files/fermilab-tm-2016.PDF
15. Ahrens, L., et al.: Development of a stepwise ray-tracing based on-line model at the AGS. WEP141, Proceedings of 2011 Particle Accelerator Conference, New York, NY, USA.
https://accelconf.web.cern.ch/PAC2011/papers/wep141.pdf
16. Leleux, G.: Compléments sur la Physique des Accélérateurs. DEA "Physique et Technologie des Grands Instruments", Université Paris VI. Rapport interne LNS//86-101, CEA Saclay (1986)
17. Leleux, G.: Synchrotron radiation. DEA "Physique et Technologie des Grands Instruments", Université Paris VI. Rapport interne LNS, CEA Saclay (1991)
18. F. Méot, et al.: Beam dynamics validation of the Halbach Technology FFAG Cell for Cornell-BNL Energy Recovery Linac. Nuclear Inst. and Methods in Physics Research, A 896 (2018) 60âĂŞ67
19. Leleux, G.: Accélérateurs Circulaires. INSTN lectures, internal report CEA Saclay (1978), unpublished
20. The 20 Years of the Synchrotron SATURNE-2. In: Proceedings of the Colloquium, Paris, France, 04 - 05 May 1998, A. Boudard and P.-A. Chamouard Editors. Edited By CEA -